

MIT Open Access Articles

Biological-Templating of a Segregating Binary Alloy for Nanowire-Like Phase-Change Materials and Memory

The MIT Faculty has made this article openly available. **Please share** how this access benefits you. Your story matters.

Citation: Loke, Desmond K. et al. "Biological-Templating of a Segregating Binary Alloy for Nanowire-Like Phase-Change Materials and Memory." ACS applied materials & interfaces 1 (2018): 6556-6562 © 2018 The Author(s)

As Published: 10.1021/acsanm.8b01508

Publisher: American Chemical Society (ACS)

Persistent URL: <https://hdl.handle.net/1721.1/124837>

Version: Author's final manuscript: final author's manuscript post peer review, without publisher's formatting or copy editing

Terms of Use: Article is made available in accordance with the publisher's policy and may be subject to US copyright law. Please refer to the publisher's site for terms of use.



Biological-Templating of a Segregating Binary Alloy for Nanowire-Like Phase-Change Materials and Memory

Desmond K. Loke,^{*,†,‡,§} Griffin J. Clausen,^{‡,||} Jacqueline F. Ohmura,^{‡,||} Tow-Chong Chong,[§] and Angela M. Belcher^{*,†,‡,||}

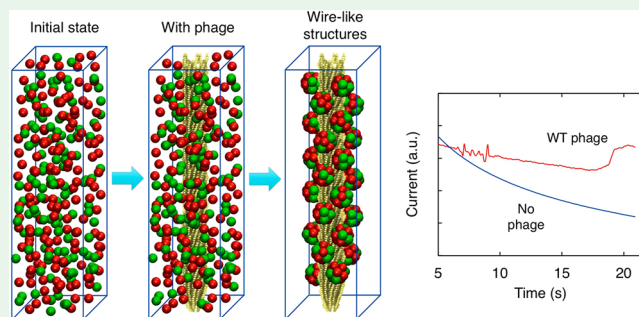
[†]Department of Materials Science and Engineering, [‡]The David H. Koch Institute for Integrative Cancer Research, and ^{||}Department of Biological Engineering, Massachusetts Institute of Technology (MIT), Cambridge, Massachusetts 02139, United States

[§]Department of Science and Math, Singapore University of Technology and Design, Singapore 487372, Singapore

Supporting Information

ABSTRACT: One of the best strategies for achieving faster computers is to mitigate the millisecond-order time delays arising from the transfer and storage of information between silicon- and magnetic-based memories. Segregating-binary-alloy (SBA)-type phase-change materials (PCMs), such as gallium antimonide-based systems, can store information on 10 ns time scales by using a single memory structure; however, these materials are hindered by the high consumption of energies and undergo elemental segregation around 620 K. Nanowire-like PCMs can achieve low-energy consumption but are often synthesized by vapor–liquid–solid methods above 720 K, which would cause irreversible corruption of SBA-based PCMs. Here we control the morphology, composition, and functionality of SBA-type germanium–tin oxide systems using template-driven nucleation that leverages the electrostatic-binding specificity of the M13 bacteriophage surface. A wirelike PCM was achieved, with controllable and reliable phase-changing signatures, capable of tens of nanoseconds switching times. This approach addresses some of the critical material compositional and structural constraints that currently diminish the utility of PCMs in universal memory systems.

KEYWORDS: phase-change materials, nanowires, switches, genetic engineering, M13 bacteriophage



INTRODUCTION

The ever-increasing demand for faster and more efficient computers has driven the widespread search for next-generation optoelectronic, photonic, or electronic memory devices that can rapidly process and store information.^{1–3} This search has been not just about exploring new methods to construct smaller or stackable systems but also about discovering novel materials or structures to integrate more devices (or perform multiple computations) on a single chip.⁴ For instance, current computers often rely on frequent information transfer between the fast, yet volatile, silicon-based random access memory (RAM) and the slow, yet nonvolatile, magnetic-based hard disk drive, transfers that typically yield delays on the order of milliseconds.⁵ To overcome this problem, one of the best solutions is to develop a single “universal-like” memory type that is both fast and nonvolatile, but this is largely unachievable using traditional silicon memories and magnetic drives.⁶

Phase-change materials (PCMs) have been shown to be excellent candidates for achieving universal memory systems, with switching times on the order of ten of nanoseconds.⁷ PCMs are based on the reversible transition between amorphous and crystalline states exhibiting altered physical

properties, viz., optical reflectance and electrical conductance.⁸ The conventional PCM, Ge₂Sb₂Te₅ (GST), can be limited by the segregation of atomic components, variation in stoichiometry, and incompatibility with complementary metal oxide semiconductor (CMOS) manufacturing processes.⁹ Tellurium-free or segregating-binary-alloy (SBA)-based materials, e.g., germanium–tin-based systems, can offer an alternative solution for realizing PCMs while avoiding the reliability and cost drawbacks of GST.¹⁰ Compared to GST, these SBA-based materials can achieve around 30% higher resistance to spontaneous crystallization during the long-term retention of information and ~10 times faster switching.¹¹ Nevertheless, SBA-type materials tend to be inhibited by high power consumption and element segregation around 620 K, making them difficult to incorporate into current integrated circuits.¹⁰

Nanowire systems are a promising strategy for achieving low power consumption in PCMs.¹² Nanowire PCMs can easily achieve sublithographic sizes, with negligible process-induced material damage due to a facile etch-free process.¹³ The

Received: August 30, 2018

Accepted: November 12, 2018

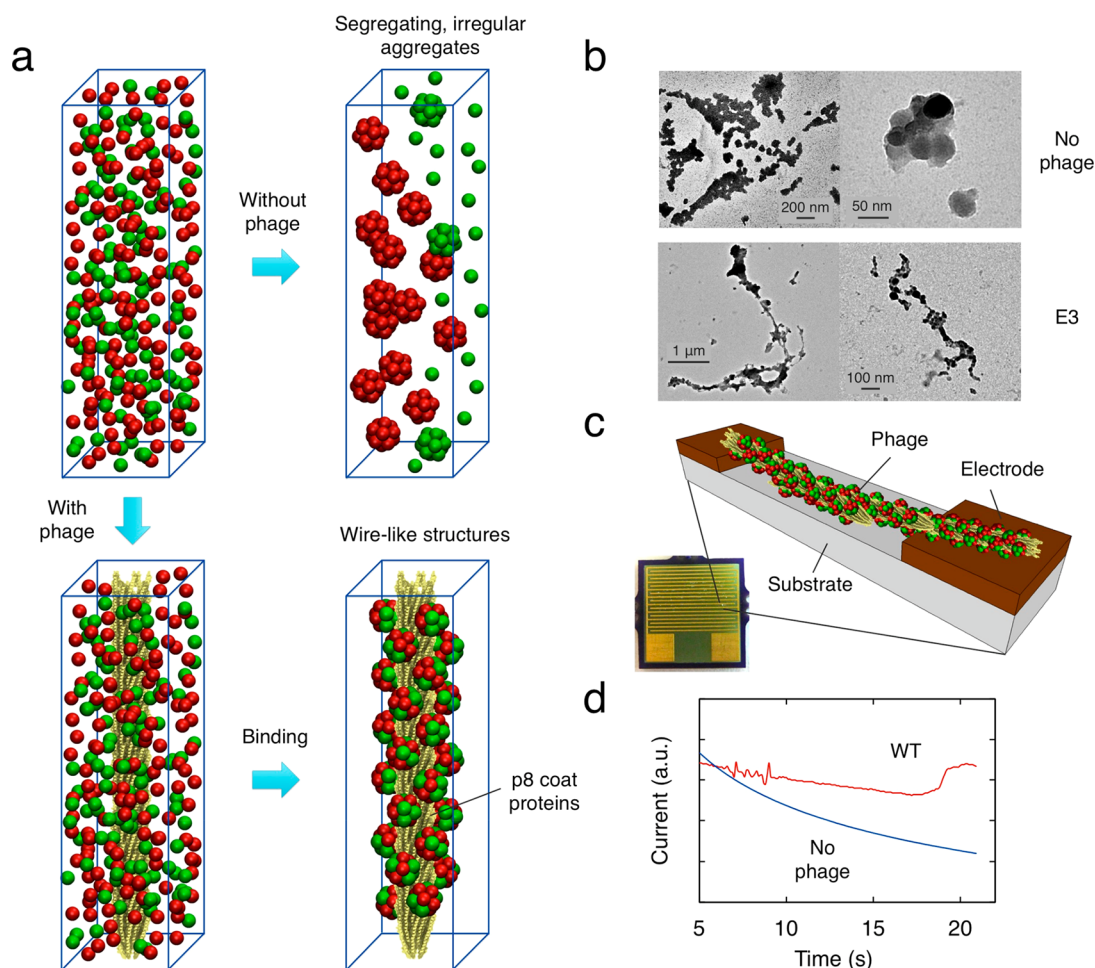


Figure 1. Binding, synthesis, and utility of the nanoscale, wirelike PCMs with phage. (a) Schematic configurations illustrating the atomic binding of materials during synthesis with and without phage. The red and green atoms represent two different species of a SBA-based material, and the yellow filaments (or wires) denote the phage. (b) TEM images of the sample of suspensions with no phage (top) and E3 phage (bottom). (c) Schematic of the test structure and also a photograph of the structure made of gold/nickel-on-copper electrodes patterned on plastic-laminated substrates. (d) Time evolution of the current that has passed through the structure with no phage and WT phage during pulsed excitations with $V \approx 8.0$ V. We have investigated multiple samples, although a sample is shown. The structure was initially at the high resistance level.

nanowires can also be constructed along the z direction for integration into advanced 3D electronic circuits.¹⁴ The switching times for Reset (crystalline to amorphous state) for some nanowire PCMs, e.g., InSbTe- and Ga-doped-InO types, can be fast, on the order of ten of nanoseconds to hundreds of nanoseconds.^{15–17} The switching times for Set (amorphous to crystalline state) can be on the order of ten of nanoseconds to a few microseconds.^{15–17} Most phase-change nanowires have been synthesized using conventional gold-catalyzed vapor–liquid–solid (VLS) processes; however, the VLS is a high-temperature process, and this method often requires heating of the Au-PCM alloy above its eutectic/melting point of around 720 K.¹⁸ A difficulty arises from the trade-off between increasing the velocity of growth and, at the same time, reducing the annealing temperature to avoid segregation of the SBA-based materials.¹⁹ Nanowire PCMs can also be grown at lower temperatures, e.g., InSbTe-based nanowires grown using the metal–organic chemical vapor deposition (MOCVD) and MOCVD-via-VLS methods at ~ 520 and 620 K, respectively, as reported recently.^{15,16}

Here, we demonstrate control of the morphology, composition, and functionality of an SBA-type PCM, germanium–tin oxide, using template-directed nucleation

achieved via electrostatic binding selectivity of the filamentous M13 bacteriophage surface. The template structure, M13 bacteriophage (“phage”), is approximately 6.5 nm in diameter and 880 nm in length and has been previously demonstrated to be an excellent biological template for achieving ultrasmall, functional wires to form self-assembly building blocks for state-of-the-art electronic devices.²⁰ The PCM can be synthesized on the M13 bacteriophage because of affinity binding between the PCM precursor components and negatively charged amino acids on the M13 bacteriophage surface. Furthermore, this platform enabled a comparison of the material composition and performance of PCMs templated on wild-type (WT) phage or a phage variant (E3) genetically engineered to have increased surface negativity.

The as-formed state of material templated on phage was observed to show a crystalline mixture due to the nucleation and growth of different germanium and tin suspension components. The crystalline mixture included germanium–tin oxide, which can function as a PCM. A similar material, gallium–indium oxide, has recently been demonstrated to show reversible switching between the crystalline and amorphous states, produced by Joule heating by applying electrical pulses.²¹ Annealing germanium–tin oxide in the

crystalline state above the melting point by an applied voltage or optical pulse can produce liquid germanium–tin oxide with a homogeneous composition. During cooling, the liquid can rapidly cool to quench it to an amorphous state (Reset process). To switch back to the crystalline state, the material can be reannealed above the crystalline temperature with an electrical or optical pulse of lower magnitude and extended duration (Set process), facilitating its atoms to rearrange into the crystalline state. We noted that the as-formed state of the sample without phage showed a crystalline mixture comprising mainly single-metal-oxide components. The sample without phage can exhibit a higher resistance level compared to the sample with phage, and it cannot show reversible switching because negligible germanium–tin oxide was produced. Pure tin oxide, for instance, has been reported to show a higher resistivity value than germanium–tin oxide.²²

Overall, a biologically templated, wirelike PCM was achieved, with tunable and reliable memory switching characteristics. We further demonstrate that by varying the amino acid composition of the phage surface, thus increasing the negativity of the template surface, the composition of the material could be controlled. Optical characterizations and binding assays revealed the specificity of phage for binding the phase-change-based precursors, which is observed to be the key to enhancing the switching signatures. This approach avoids the high-energy synthesis of material systems and atomic segregation of initial material phases by using low-temperature templated nucleation kinetics rather than the thermally expensive VLS dynamics.

RESULTS AND DISCUSSION

The germanium–tin oxide suspension was synthesized by mixing phage in GeCl_4 and $\text{SnCl}_4 \cdot 5\text{H}_2\text{O}$ precursor solutions at 277 K (see the Experimental Section in the Supporting Information). To assess the effect of the phage surface chemistry on the synthesis of nanowire-like structures, two M13 phage variants, WT and E3, were compared. The body (capsid) of the M13 phage is composed of approximately 2700 copies of the p8 major coat protein, with several additional coat proteins comprising the phage termini.²³ The E3 phage is a modified clone of the WT M13KE phage, with an additional negatively charged amino acid incorporated into each p8 coat protein.²⁴ This is achieved by replacing the WT peptide sequence EGD with the triglutamate EEE within the solvent-exposed terminus of the p8 protein. Because of the presence of additional carboxylic acid groups compared to the WT proteins, the E3 phage exhibits stronger ionic interactions with cations, which can promote the binding between a target material and phage and drive nucleation of the target material on phage surfaces²⁵ (Figure 1a).

By transmission electron microscopy (TEM) inspection, the suspension without phage showed irregular material aggregates, in marked contrast to the suspension with WT or E3 phage, which showed dispersions with wirelike structures, indicating that the morphology of PCMs can be modified by different suspension components (Figures 1b and S1). Silicon-based nanowires have been demonstrated to exhibit less regular forms and sub-50-nm thicknesses for achieving 3D integrated circuits.²⁶ Phage-templated samples also showed wirelike configurations with lower homogeneity and several tens of nanometers thickness, integrable with 3D circuitries, viz., around 45 nm. It should be noted that such low-temperature (viz., ~ 277 K), line-type structures were not

facilely realized by previous VLS studies, which typically require temperatures above 720 K.¹⁹ These findings illustrate the facility of the biological-based methodology to achieve nanometer-sized, wire-based configurations of PCMs at low temperature.

Energy-dispersive X-ray spectroscopy (EDS) mapping was used to obtain the distribution of germanium and tin for the PCM suspension with and without a phage template. Nontemplated suspensions contained irregular clusters composed of a high amount of germanium, with a negligible amount of tin (Figure 2a). This is in marked contrast to phage-

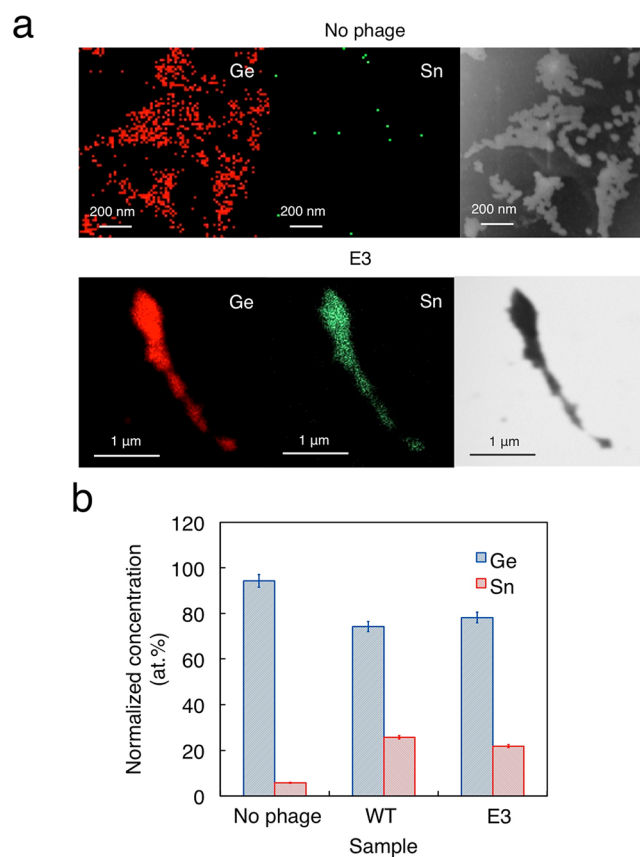


Figure 2. Control and tuning of the components of the PCM via phage-enabled binding. (a) EDS mapping of the sample of suspensions with no phage and E3 phage. Color coding of atomic species: Ge, red; Sn, green. The TEM image of the sample is also shown (right). (b) Dependence of the normalized species concentration on the phage used for the samples. The species concentration was estimated using a simple calculation, e.g., (amount of germanium or tin/total amount of germanium and tin) \times 100%. The error bars show the range of values obtained from experiments performed on two different samples.

templated samples, which showed high amounts of both germanium and tin (Figures 2a and S2). Figure 2b shows the normalized concentration values of germanium and tin for the suspension with and without phage, i.e., (amount of germanium or tin/total amount of germanium and tin) \times 100%. The phage-templated systems showed a higher concentration of tin compared to the nontemplated system, viz., about ~ 21.8 – 25.7 and 5.7 atom %. The E3 phage-templated system exhibited an increased concentration of germanium relative to the WT phage-templated system, viz., 78.1 and 74.2 atom %, implying that the concentration of the

PCMs can be manipulated by varying the phage surfaces. Additionally, the E3 phage-templated samples showed uniform distributions of germanium and tin (Figure 2a). Figure S7 also details the components of the samples. We note that such uniformity of germanium and tin is not easily achieved by previous studies of germanium–tin clusters/ions implanted within silica matrixes, which require high-temperature ion implantation, causing elemental segregation of the initial material state.¹⁰ A difficulty arises from the trade-off between lowering the energy needed for injecting ions and increasing the depth of penetration beyond the material surface.²⁷

To investigate how WT and E3 phages were capable of templating PCMs with different concentrations of Ge and Sn under the same synthesis conditions, a binding affinity experiment was conducted on both bulk samples and the Ge and Sn precursor materials. Using an enzyme-linked immunosorbent assay (see the Experimental Section in the Supporting Information), we have found that the E3 phage can bind Ge more readily than the WT phage, while both phage variants have similar affinities to Sn (Figure 3a). Moreover, we investigated the specificity of phage for binding the phase-change-based precursors by examining the suspension with

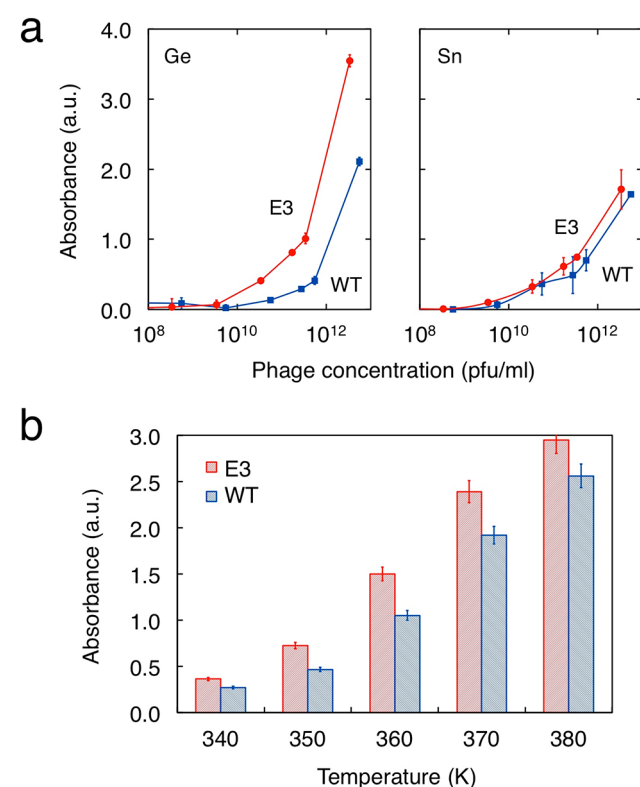


Figure 3. Investigation of the mechanism and characteristics of the phage-enabled binding for the PCMs. (a) Plots showing the absorbance values for the metal-bound phage sample measured using the horseradish peroxidase-conjugated anti-M13 antibody with a colorimetric substrate for varying the phage concentrations. The absorbance of the sample was measured at $\lambda \approx 450$ nm. (b) Dependence of the absorbance values for the suspension with phage on the synthesis temperatures. The absorbance values were obtained from UV–vis absorption spectroscopy spectra of the suspension measured at $\lambda \sim 700$ nm (Figure S3). The suspension was heated for 15 min before each spectrum measurement. The error bars show the range of values obtained from experiments performed on two different samples/suspensions.

phage after incorporating the last precursor (see the Experimental Section in the Supporting Information). The suspension with phage of high affinity to oxide-based materials has been shown to display higher absorbance values relative to the suspension with a low-oxide-affinity phage.²⁸ By ultraviolet–visible (UV–vis) absorption spectroscopy, the suspension with E3 phage showed higher absorbance versus the suspension with WT phage for varying synthesis temperatures (Figure 3b). The same result is similarly observed for alternate synthesis durations (Figure S4). These results agree with those in Figure 2 and indicate that the E3 phage has a higher preference for binding the PCMs than the WT phage. The findings further suggest that the selectivity of phage for binding these materials is robust to both variations in time and temperature.

For the first time, we have shown a phase-change-based, biologically enabled, switchable material with fast switching characteristics. Our PCM suspensions were cast upon Au/Ni-on-Cu patterned electrode arrays to construct metal-to-phage-templated-materials-to-metal testable configurations, concomitant with the testing setup for other curli-based systems²⁹ (Figure 1c). The samples were initially at the high resistance level. Voltage pulses were applied to tune the resistance state of the samples, and the resulting conductivities were measured. Upon electrical pulse excitation, configurations without biological templating showed no increase in conductance from the high resistance state (Figure 1d). In contrast, the WT phage-templated samples showed marked increase in the electrical conductivity. Furthermore, various voltage magnitudes and pulse lengths were delivered and the resulting steady-state resistances measured. Nontemplated systems could not be switched from the high to low resistance levels (Set), let alone back to the starting level (Reset), compared to the templated configurations, which can perform both operations, viz., between ~ 20 and 5 M Ω , suggesting that the functionality of PCMs can be controlled by altering the suspension components (Figure 4a,b). In comparison, gallium–indium-based phase-change alloys have been demonstrated to display reversible switching between the high and low resistance levels on the order of several tens of megaohms and megaohms, respectively.²¹

A Set transition is normally slower than Reset, thus limiting the overall PCM speed.¹¹ By optical pulse excitation, we found that the E3-templated PCM can exhibit Set with pulses on the order of tens of nanoseconds, viz., ~ 90 ns (Figure S6), which is promising compared with those for advanced solution-based phase-change films, viz., GeSbSe with 100-ns-order switching pulses.³⁰ The combined use of X-ray diffraction (XRD), current–voltage, and resistance–voltage measurements further infers that the E3-templated configurations should exhibit switching from the amorphous-and-crystalline state to the crystalline/intermediate state before and after the Set process (Figures S7–S10).

Interesting aspects of organic-template-derived materials with alterable and reliable signatures for memory applications have been reported in the literature. Poly(vinylidene fluoride-co-trifluoroethylene) (PVDF-TrFE) memory structures have been demonstrated to show switching voltage and switching times for Set in the few volts range and more than 1 s range, respectively.³¹ Researchers have also reported that germanium telluride nanoparticle (GeTe-NP)-based memory structures exhibit switching bias and switching duration for Set on the order of several volts and hundreds of microseconds,

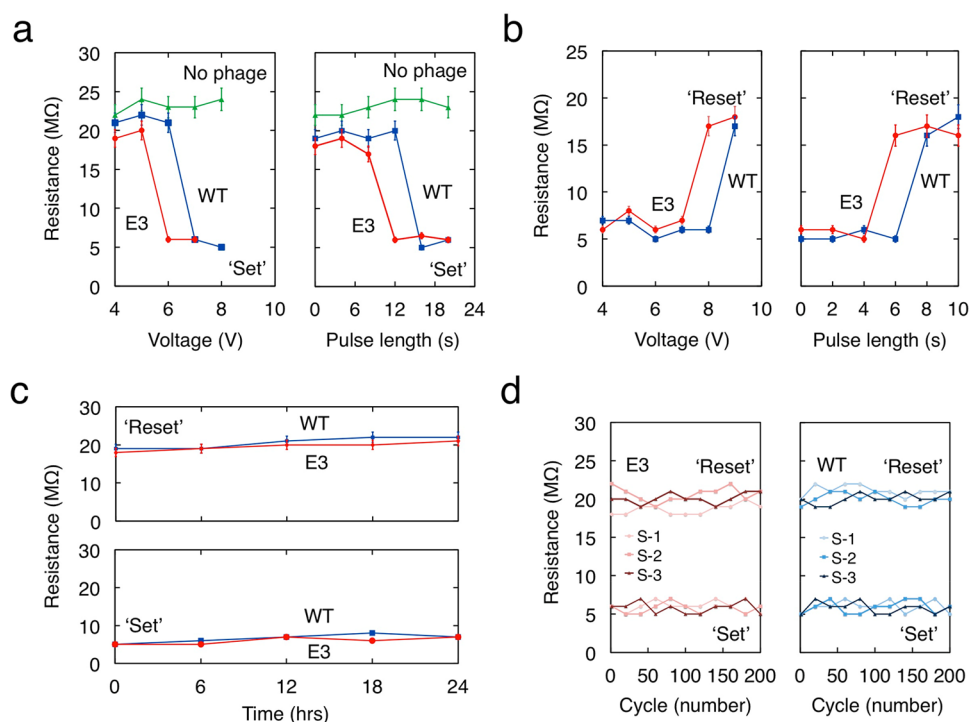


Figure 4. Phage-templated PCM structures exhibiting controllable and reliable switching characteristics. Dependence of the applied voltage pulse magnitude (left) and duration (right) on the (a) Set and (b) Reset processes. A fixed pulse duration (~ 20 s) was maintained during the testing of different voltage pulse magnitudes. Fixed voltages of around 7.0 and 9.0 V were maintained while testing pulse durations for the Set and Reset operations, respectively. (c) Time evolution of the device resistance for the device in the high (top) and low (bottom) resistance levels. (d) Repeated device switching between high and low resistance states, for both WT and E3 phage-templated PCMs. In parts a–c, the error bars show the range of values obtained from experiments performed on 10, 10, and 3 different devices, respectively. In part d, the number of samples was $n = 3$. In parts a–d, the device was switched between the high and low resistance levels of $R \approx 20$ and 5 $M\Omega$, respectively.

respectively.³² These structures (GeTe-NP) also show switching voltage and switching times for Reset are on the order of tens of volts and tens of nanoseconds, respectively.³² Our E3 phage-templated PCM systems displayed lower switching voltages and faster switching times for Set relative to the WT phage-templated systems, e.g., around 6.0 and 7.0 V and ~ 12 and 16 s, respectively (Figure 4a). A similar enhancement in the same set of parameters is further noted for Reset, i.e., approximately 8.0 and 9.0 V and ~ 6 and 8 s (Figure 4b). Additionally, PVDF-TrFE/GeTe-NP systems have demonstrated the retention of alternate electrical conductance levels on the order of several hours and reversible switching between the high and low resistance levels on the order of tens to hundreds of cycles.^{31,32} As predicted, the nontemplated structure could not achieve long retention of both high or low resistance levels and good reversibility of switching between these levels; it effectively remains at the high resistance state (Figure S11). In contrast, the phage-templated systems could achieve all of these functions, meaning that the functionality of PCMs is robust to modifications in time and electrical excitation, viz., more than 24 h and >200 cycles (Figure 4c,d).

Furthermore, the phage-templated configurations can show faster speed for Set with electrical priming,³³ viz., around 95 ns (Figure S12). Similarly, the switching time for Reset becomes shorter with electrical premelting,³⁴ e.g., less than ~ 60 – 70 ns. It should be noted that the phage-templated configurations show a decreased programming window, e.g., from a factor of ~ 100 (Figure S10; around 20 $M\Omega$ to 200 $k\Omega$) to a factor of 4 (Figure 4a,b; ~ 20 to 5 $M\Omega$), when the pulse length is decreased from around 90 s (Figure S10) to 20 s (Figure

4a,b).³⁵ Under nanosecond pulse treatment, the window might be reduced such that it becomes effectively undetectable. However, with electrical priming, the programming window of approximately 20 $M\Omega$ to 200 $k\Omega$ can be preserved by using a ~ 95 ns pulse (Figure S12). It may be that some thermal prestructural ordering is induced by electrical priming, enabling faster nucleation and growth upon a subsequent stronger electrical pulse. We note that the switching voltages, speeds, cycles, and retention-times achieved in our structures (E3) may be less enhanced compared to those for other traditional high-temperature PCM syntheses.¹⁸ We believe that through additional selection and genetic engineering we will continue to advance targeted device characteristics including switching voltage, speed, cycle, and retention time.

The germanium–tin oxide related materials templated on phage demonstrate switching behavior that we attribute to germanium–tin oxide. However, other components, e.g., GeO_2 and $GeSn$, might also contribute to this behavior. We are limited in our ability to quantify the ratio of these species, i.e., $GeSnO$, GeO_2 , and $GeSn$, in specific nanowires because it can be generally difficult to use typical atomic composition measurements, e.g., EDS mapping, to distinguish an element between particular species.³⁶ Given the synthesis and casting of the nanowires onto the device electrodes, it can be reasonable that not all nanowires make contact with the electrodes and thus not all nanowires undergo phase transition. However, it should be noted that multiple nanowire devices show reproducible characteristics for the same phage type in 3–10 devices for all Set and Reset experiments (Figures 4 and S6, S9,

S10, and S12), indicating that the sample preparation might not significantly affect the performance reproducibility.

The primary focus of this work is to demonstrate the feasibility of low-temperature synthesis and control of the PCM composition through filamentous phage surface charge. The optical, material, and electrical characterization results suggest that the controllable and reliable switching characteristics derive from the specificity of electrostatic binding during synthesis. By synthesis of a material using phage with a stronger affinity for phase-change-based precursors, a systematic increase in the uniformity of atomic distributions could facilitate the atomic diffusion necessary for the alternate forms of structural ordering during switching. This phenomenon would explain both the observed controllable switching and reliable properties seen in the structure with phage. For the purpose of investigating the effect of size, which is another important variable that can affect the PCM performance,³⁷ future work should include modulation of the length of the M13 phage³⁸ or the use of alternative biological templates with different aspect ratios, e.g., tobacco mosaic virus, 18 nm in diameter and 300 nm in length.³⁹

In this work, we employed a filamentous bacteriophage as a nucleation template to enable a low-temperature synthesis of a wirelike PCM that demonstrated tunable and reliable switching signatures. The improved species distributions, switching voltages, and switching times realized by the E3 phage over the WT phage imply that advanced genetic engineering of the template phage, whether through rational design or directed evolution, has the ability to further enhance these PCM characteristics. In addition, the modular nature of the M13 phage could be leveraged to add orthogonal functionalities to the system for achieving avant-garde self-assembly electronic circuits. One such scheme might be to engineer the p3- and p9-coated proteins at the ends of the phage to express peptides with binding specificity for titanium nitride, a widely used CMOS-compatible material. This could not only facilitate connection of the templated PCM to external circuitry but also assist controlled placement to a specific location on the semiconductor substrate, thus opening new opportunities for optimizing the performance of wirelike, phase-change, non-volatile memory devices.

■ ASSOCIATED CONTENT

📄 Supporting Information

The Supporting Information is available free of charge on the ACS Publications website at DOI: 10.1021/acsanm.8b01508.

Experimental procedures, material-structure discussion, and characterization data (PDF)

■ AUTHOR INFORMATION

Corresponding Authors

*E-mail: desmond_loke@sutd.edu.sg

*E-mail: belcher@mit.edu

ORCID

Desmond K. Loke: 0000-0001-5799-6441

Angela M. Belcher: 0000-0001-9353-7453

Notes

The authors declare no competing financial interest.

■ ACKNOWLEDGMENTS

The authors thank W. J. Wang, L. Li, M. H. Li, W. D. Song, and Y. Zhang for invaluable help on the material/device characterization studies and J. Qi and S. A. Steiner for fruitful insights on the biological/chemical synthesis investigations. We thank The David H. Koch Institute for Integrative Cancer Research for use of their facilities to synthesize and characterize the test suspensions. The material characterizations were performed using the MIT Center for Materials Science and Engineering Facility and SUTD Material Characterization Design Lab. D.K.L. thanks the Singapore University of Technology and Design and Ministry of Education for financial support.

■ REFERENCES

- (1) Hosseini, P.; Wright, C. D.; Bhaskaran, H. An Optoelectronic Framework Enabled by Low-Dimensional Phase-Change Films. *Nature* **2014**, *511*, 206–211.
- (2) Hu, L.; Yuan, J.; Ren, Y.; Wang, Y.; Yang, J. Q.; Zhou, Y.; Zeng, Y. J.; Han, S. T.; Ruan, S. Phosphorene/ZnO Nano-Heterojunctions for Broadband Photonic Nonvolatile Memory Applications. *Adv. Mater.* **2018**, *30*, 1801232.
- (3) Yu, G.; Upadhyaya, P.; Shao, Q.; Wu, H.; Yin, G.; Li, X.; He, C.; Jiang, W.; Han, X.; Amiri, P. K.; Wang, K. L. Room-Temperature Skyrmion Shift Device for Memory Application. *Nano Lett.* **2017**, *17*, 261–268.
- (4) Johnson, R. C. Intel Plans a Future of CMOS Technology. http://www.eetimes.com/document.asp?doc_id=1329353 (Accessed July 10, 2018).
- (5) Kryder, M. H.; Kim, C. S. After hard drives—What comes next? *IEEE Trans. Magn.* **2009**, *45*, 3406–3413.
- (6) Perniola, L.; Molas, G.; Navarro, G.; Nowak, E.; Sousa, V.; Vianello, E.; De Salvo, B. Universal Signatures from Non-Universal Memories: Clues for the Future. *IEEE 8th International Memory Workshop* **2016**, 1–3.
- (7) Xiong, F.; Liao, A. D.; Estrada, D.; Pop, E. Low-Power Switching of Phase-Change Materials with Carbon Nanotube Electrodes. *Science* **2011**, *332*, 568–570.
- (8) Ovshinsky, S. R. Reversible Electrical Switching Phenomena in Disordered Structures. *Phys. Rev. Lett.* **1968**, *21*, 1450–1453.
- (9) Chen, Y.; Wang, G.; Shen, X.; Xu, T.; Wang, R. P.; Wu, L.; Lu, Y.; Li, J.; Dai, S.; Nie, Q. Crystallization Behaviors of Zn_xSb_{100-x} Thin Films for Ultralong Data Retention Phase Change Memory Applications. *CrystEngComm* **2014**, *16*, 757–762.
- (10) Shin, S. J.; Guzman, J.; Yuan, C. W.; Liao, C. Y.; Boswell-Koller, C. N.; Stone, P. R.; Dubon, O. D.; Minor, A. M.; Watanabe, M.; Beeman, J. W.; Yu, K. M.; Ager, J. W.; Chrzan, D. C.; Haller, E. E. Embedded Binary Eutectic Alloy Nanostructures: A New Class of Phase Change Materials. *Nano Lett.* **2010**, *10*, 2794–2798.
- (11) Lu, Y.; Song, S.; Song, Z.; Liu, B. Ga₁₄Sb₈₆ Film for Ultralong Data Retention Phase-Change Memory. *J. Appl. Phys.* **2011**, *109*, 064503.
- (12) Lee, S.-H.; Jung, Y.; Agarwal, R. Highly Scalable Non-Volatile and Ultra-Low-Power Phase-Change Nanowire Memory. *Nat. Nanotechnol.* **2007**, *2*, 626–630.
- (13) Meister, S.; Peng, H.; McIlwrath, K.; Jarausch, K.; Zhang, X. F.; Cui, Y. Synthesis and Characterization of Phase-Change Nanowires. *Nano Lett.* **2006**, *6*, 1514–1517.
- (14) Muneer, S.; Gokirmak, A.; Silva, H. Vacuum-Insulated Self-Aligned Nanowire Phase-Change Memory Devices. *IEEE Trans. Electron Devices* **2015**, *62*, 1668–1671.
- (15) Ahn, J. K.; Park, K. W.; Jung, H. J.; Yoon, S. G. Phase-Change InSbTe Nanowires Grown in Situ at Low Temperature by Metal–Organic Chemical Vapor Deposition. *Nano Lett.* **2010**, *10*, 472–477.
- (16) Selmo, S.; Cecchini, R.; Cecchi, S.; Wiemer, C.; Fanciulli, M.; Rotunno, E.; Lazzarini, L.; Rigato, M.; Pogany, D.; Lugstein, A.

Longo, M. Low Power Phase Change Memory Switching of Ultra-Thin $\text{In}_3\text{Sb}_1\text{Te}_2$ nanowires. *Appl. Phys. Lett.* **2016**, *109*, 213103.

(17) Jin, B.; Lim, T.; Ju, S.; Latypov, M. I.; Kim, H. S.; Meyyappan, M.; Lee, J. S. Ga-doped Indium Oxide Nanowire Phase Change Random Access Memory Cells. *Nanotechnology* **2014**, *25*, 055205.

(18) Yu, B.; Ju, S.; Sun, X.; Ng, G.; Nguyen, T. D.; Meyyappan, M.; Janes, D. B. Indium Selenide Nanowire Phase-Change Memory. *Appl. Phys. Lett.* **2007**, *91*, 133119.

(19) Jung, Y.; Yang, C. Y.; Lee, S. H.; Agarwal, R. Phase-Change Ge-Sb Nanowires: Synthesis, Memory Switching, and Phase-Instability. *Nano Lett.* **2009**, *9*, 2103–2108.

(20) Moradi, M.; Li, Z.; Qi, J.; Xing, W.; Xiang, K.; Chiang, Y.-M.; Belcher, A. M. Improving the Capacity of Sodium Ion Battery Using a Virus-Templated Nanostructured Composite Cathode. *Nano Lett.* **2015**, *15*, 2917–2921.

(21) Wang, S.-L.; Peng, L.-H. Phase-Change Activities on Gallium-Doped Indium Oxide. *J. Appl. Phys.* **2010**, *108*, 084503.

(22) Arita, M.; Konishi, H.; Masuda, M.; Hayashi, Y. Effects of Protium Introduction on Electrical and Optical Properties of Tin-Germanium Oxide Thin Films. *Mater. Trans.* **2002**, *43*, 2670–2672.

(23) Oh, D.; Qi, J.; Han, B.; Zhang, G.; Carney, T. J.; Ohmura, J.; Zhang, Y.; Shao-Horn, Y.; Belcher, A. M. M13 Virus-Directed Synthesis of Nanostructured Metal Oxides for Lithium-Oxygen Batteries. *Nano Lett.* **2014**, *14*, 4837–4845.

(24) Marvin, D. A.; Hale, R. D.; Nave, C.; Citterich, M. H. Molecular Models and Structural Comparisons of Native and Mutant Class I Filamentous Bacteriophages. *J. Mol. Biol.* **1994**, *235*, 260–286.

(25) Lee, Y. J.; Lee, Y.; Oh, D.; Chen, T.; Ceder, G.; Belcher, A. M. Biologically Activated Noble Metal Alloys at the Nanoscale: For Lithium Ion Battery Anodes. *Nano Lett.* **2010**, *10*, 2433–2440.

(26) Dupré, C.; Hubert, A.; Becu, S.; Jublot, M.; Maffini-Alvaro, V.; Vizioz, C.; Aussenac, F.; Arvet, C.; Barnola, S.; Hartmann, J. M.; Garnier, G.; et al. 15 nm-Diameter 3D Stacked Nanowires with Independent Gates Operation: Φ FET. *IEEE Int. Electron Devices Meet* **2008**, 1–4.

(27) Fraboni, B.; Scidà, A.; Cosseddu, P.; Wang, Y.; Nastasi, M.; Milita, S.; Bonfiglio, A. Turning an Organic Semiconductor into a Low-Resistance Material by Ion Implantation. *Sci. Technol. Adv. Mater.* **2015**, *16*, 065008.

(28) Żelechowska, K.; Karczewska-Golec, J.; Karczewski, J.; Łoś, M.; Klónkowski, A. M.; Węgrzyn, G.; Golec, P. Phage-Directed Synthesis of Photoluminescent Zinc Oxide Nanoparticles under Benign Conditions. *Bioconjugate Chem.* **2016**, *27*, 1999–2006.

(29) Chen, A. Y.; Deng, Z.; Billings, A. N.; Seker, U. O. S.; Lu, M. Y.; Citorik, R. J.; Zakeri, B.; Lu, T. K. Synthesis and Patterning of Tunable Multiscale Materials with Engineered Cells. *Nat. Mater.* **2014**, *13*, 515–523.

(30) Milliron, D. J.; Raoux, S.; Shelby, R. M.; Jordan-Sweet, J. Solution-Phase Deposition and Nanopatterning of GeSbSe Phase-Change Materials. *Nat. Mater.* **2007**, *6*, 352–356.

(31) Hwang, S. K.; Park, T. J.; Kim, K. L.; Cho, S. M.; Jeong, B. J.; Park, C. Organic One-Transistor-Type Nonvolatile Memory Gated with Thin Ionic Liquid-Polymer Film for Low Voltage Operation. *ACS Appl. Mater. Interfaces* **2014**, *6*, 20179–20187.

(32) Jeyasingh, R. G. D.; Caldwell, M. A.; Milliron, D. J.; Wong, H.-S. P. First Demonstration of Phase Change Memory Device Using Solution Processed GeTe Nanoparticles. *Proc. Eur. Solid-State Device Res. Conf.* **2011**, 99–102.

(33) Loke, D.; Lee, T. H.; Wang, W. J.; Shi, L. P.; Zhao, R.; Yeo, Y. C.; Chong, T. C.; Elliott, S. R. Breaking the Speed Limits of Phase-Change Memory. *Science* **2012**, *336*, 1566–1569.

(34) Loke, D.; Skelton, J. M.; Wang, W. J.; Lee, T. H.; Zhao, R.; Chong, T. C.; Elliott, S. R. Ultrafast Phase-Change Logic Device Driven by Melting Processes. *Proc. Natl. Acad. Sci. U. S. A.* **2014**, *111*, 13272–13277.

(35) Nirschl, T.; Philipp, J. B.; Happ, T. D.; Burr, G. W.; Rajendran, B.; Lee, M. H.; Schrott, A.; Yang, M.; Breitwisch, M.; Chen, C. F.; Joseph, E.; et al. Write Strategies for 2 and 4-Bit Multi-Level Phase-

Change Memory. *IEEE International Electron Devices Meeting Technol. Digest* **2007**, 461–464.

(36) Pirrie, D.; Power, M. R.; Rollinson, G. K.; Wiltshire, P. E. J.; Newberry, J.; Campbell, H. E. Automated SEM-EDS (QEMSCAN®) Mineral Analysis in Forensic Soil Investigations: Testing Instrumental Reproducibility. *Criminal and Environmental Soil Forensics*; Springer: Dordrecht, The Netherlands, 2009; pp 411–430.

(37) Zheng, Q.; Wang, Y.; Zhu, J. Nanoscale Phase-Change Materials and Devices. *J. Phys. D: Appl. Phys.* **2017**, *50*, 243002.

(38) Rakonjac, J.; Feng, J. N.; Model, P. Filamentous Phage are Released from the Bacterial Membrane by a Two-Step Mechanism Involving a Short C-Terminal Fragment of pIII. *J. Mol. Biol.* **1999**, *289*, 1253–1265.

(39) Dujardin, E.; Peet, C.; Stubbs, G.; Culver, J. N.; Mann, S. Organization of Metallic Nanoparticles Using Tobacco Mosaic Virus Templates. *Nano Lett.* **2003**, *3*, 413–417.